THE JOURNAL OF PHYSICAL CHEMISTRY LETTERS
A JOURNAL OF THE AMERICAN CHEMICAL SOCIETY

pubs.acs.org/JPCL

Letter

Atomistic Insights Into the Degradation of Inorganic Halide Perovskite $CsPbI_3$: A Reactive Force Field Molecular Dynamics Study

Mike Pols, José Manuel Vicent-Luna, Ivo Filot, Adri C. T. van Duin, and Shuxia Tao*

Cite This: *J. Phys. Chem. Lett.* 2021, 12, 5519–5525

Read Online

ACCESS | Metrics & More | Article Recommendations | Supporting Information

ABSTRACT: Halide perovskites make efficient solar cells but suffer from several stability issues. The characterization of these degradation processes is challenging because of the limited spatiotemporal resolution in experiments and the absence of efficient computational methods to study these reactive processes. Here, we present the first reactive force field for molecular dynamics simulations of the phase instability and the defect-induced degradation in $CsPbI_3$. We find that the phase transitions are driven by the anharmonic fluctuations of the atoms in the perovskite lattice. At low temperatures, the Cs cations tend to move away from their preferential positions, resulting in worse contacts with the surrounding metal halide framework which initiates the conversion to a nonperovskite phase. Moreover, our simulations of defective structures reveal that, although both iodine vacancies and interstitials are mobile in the perovskite lattice, the vacancies have a detrimental effect on the stability, leading to the decomposition of perovskites to PbI_2.

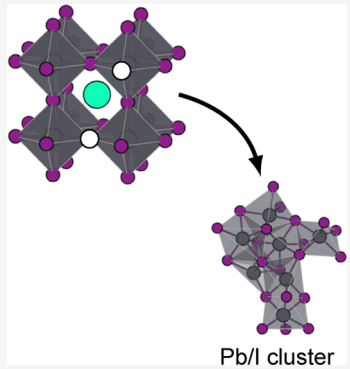

In the past decade, halide perovskites have emerged as a promising alternative to silicon for solar cells due to their exceptional optoelectronic properties and facile fabrication methods.[1,2] Despite a considerable increase in the performance of perovskite solar cells (PSCs), evidenced by their increase in their efficiency from 3.8% in 2009[3] to over 25% in 2020,[4] the commercialization of perovskite solar cells is hindered by their poor long-term stability. Halide perovskites have a three-dimensional structure with the AMX_3 chemical formula, where A is a monovalent inorganic or organic cation (Cs^+, methylammonium MA^+, or formamidimium FA^+), M is a divalent metal cation (Pb^{2+} or Sn^{2+}), and X is a monovalent halide anion (I^-, Br^-, or Cl^-). The metal and halide ions form a network of corner-sharing MX_6 octahedra, with the center of the cuboids formed by these octahedra occupied by the relatively large monovalent A cation. The crystal lattice is held together by a mix of ionic and relatively weak covalent bonds, as a result of which this class of materials has a soft and dynamical lattice.[5−8] Such a dynamical lattice has significant implications in both the efficiency and the long-term stability of PSCs. In particular, electron−phonon coupling has shown to directly affect the charge carrier mobility and carrier lifetime.[9]

Most of the stability issues of PSCs come from the intrinsic instability of the perovskite absorber layers.[10−13] Such instability issues include a phase instability where the perovskite transforms to a more stable nonperovskite phase, with worse optoelectronic properties and thus a decreased power conversion efficiency of the PSC.[14] Moreover, spin coating, the typical fabrication method of perovskites, introduces a large number of defects in the perovskite films,[15,16] the migration and accumulation of which is suggested to have a major impact on the long-term stability of PSCs.[17−19] While experimental studies offer a wide variety of insights at the macroscopic and mesoscopic scale, the interpretation of the atomistic details of the degradation processes is often difficult. Computer simulations can make a significant contribution to the understanding of the atomistic and microscopic mechanisms.

So far, the bulk of the computational investigations of halide perovskites has been done using computationally expensive methods based on quantum mechanics (QM),[20−22] only allowing for the simulation of short time scales and small system sizes. Molecular dynamics (MD) simulations that make use of classical force fields are an efficient means to study large systems at long time scales. One of the first classical force fields for the hybrid halide perovskite $MAPbI_3$, developed by Mattoni et al.,[23] has seen a wide range of applications, which include cation dynamics,[23] defect dynamics,[24,25] and dissolution in water.[26] However, this interatomic potential is primarily tailored to pure perovskite systems. Recently, some advances have been made in the development of potentials for mixed compositions, including the AMOEBA polarizable force field by Rathnayake et al. for hybrid ($MAPbI_3$) and inorganic ($CsPbI_3$) perovskites[27] and a potential for $CsPb(Br_xI_{1-x})_3$ by

Received: April 13, 2021
Accepted: June 2, 2021
Published: June 7, 2021

https://doi.org/10.1021/acs.jpclett.1c01192
J. Phys. Chem. Lett. 2021, 12, 5519−5525

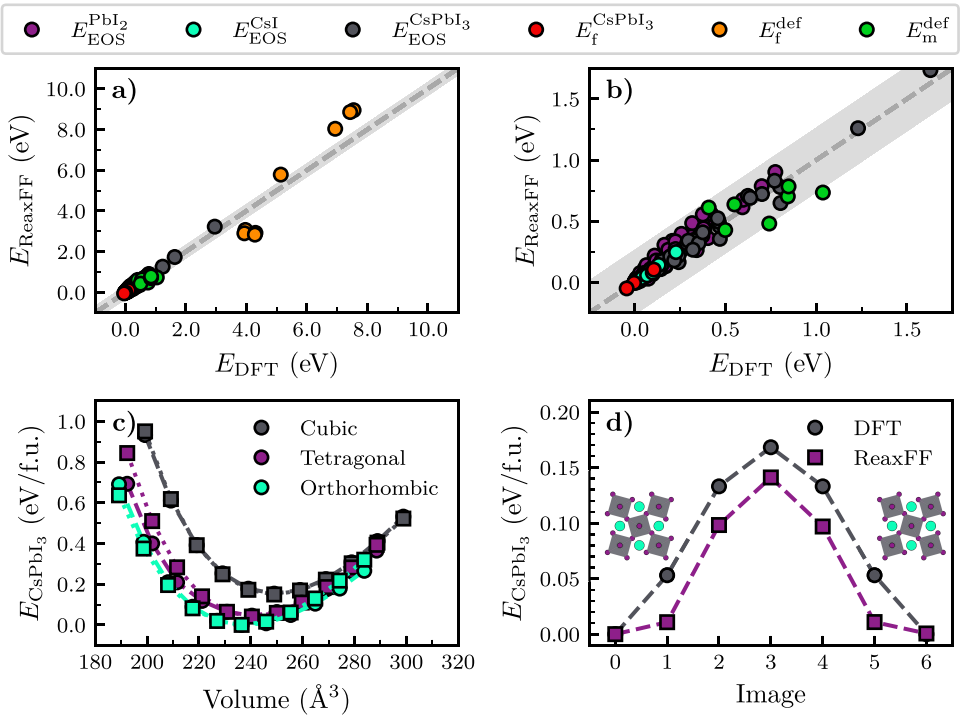

Figure 1. (a, b) Overall agreement between the prediction with the I/Pb/Cs ReaxFF force field and the reference data from DFT. (c) Comparison between the equations of state of bulk $CsPbI_3$ from DFT (circles) and ReaxFF (squares). (d) Comparison of the inversion barrier for the octahedral tilting pattern in tetragonal $CsPbI_3$ from DFT (circles) and ReaxFF (squares).

Balestra et al.[28] While these existing force fields have shown to be a powerful means to study a wide range of dynamical properties, they are unable to describe the formation and breaking of chemical bonds.

From the above, we conclude that a reactive force field (ReaxFF) interatomic potential, that employs a dynamical bond order to describe the creation and breaking of bonds,[29−31] can be a valuable computational framework to study degradation processes in halide perovskites. Here, we present the first effort toward the development of a ReaxFF force field for halide perovskites, specifically inorganic $CsPbI_3$. We obtain a set of ReaxFF parameters by training against accurate reference data from QM calculations. To demonstrate the applicability of our ReaxFF force field in investigations of dynamical and reactive processes, we perform molecular dynamics simulations to study two instability problems found in $CsPbI_3$, i.e., the phase instability and defect-accelerated decomposition. Combining analyses, such as phase diagrams, positional probability distributions, mean square displacements, and atom trajectories, we provide important atomistic insights for both degradation processes.

The ReaxFF parameters for $CsPbI_3$ were trained against a set of reference data calculated with density functional theory (DFT) with the PBE + DFT-D3(BJ) exchange-correlation functional[32−34] in the VASP software package.[35−38] The training set included different perovskite phases of $CsPbI_3$ and precursor structures (CsI and PbI_2). The calculations covered equations of state, atomic charges, formation energies, defect formation energies, and defect migration barriers (see Supporting Notes 1 and 2 in the Supporting Information for details). The parameter optimization was done with a Monte Carlo-based force field optimizer[39] as implemented in AMS 2020.[40] As a starting point for the parameter optimization, we used the Cs and I ReaxFF parameters from the electrolyte-water parameter set by Fedkin et al.[41] Without any ReaxFF parameters for Pb in the literature, we used the atomic parameters from the parametrically similar element platinum by Fantauzzi et al.,[42] which we appropriately adjusted to account for the valency and atomic mass of lead.

Following this optimization procedure, we obtained a parameter set that exhibits a good match between ReaxFF and the reference data. The optimized I/Pb/Cs ReaxFF parameters can be found in the Supporting Information. A comparison of the overall agreement between ReaxFF and the reference data is shown in Figure 1a and Figure 1b, with a more detailed overview shown in Supporting Note 3 of the SI. Generally, the ReaxFF parameter set shows a good agreement for the equations of state (E_{EOS}), perovskite formation energies ($E_f^{CsPbI_3}$), and defect migration barriers (E_m^{def}). To demonstrate the agreement, a comparison of the bulk equations of state for $CsPbI_3$ is shown in Figure 1c. In addition to the comparison to the reference data, we also carried out some validation tests to confirm that the ReaxFF parameter set has predictive power, i.e., not only describing the entries in the training set well but also capturing some material behavior not explicitly trained against. Here, we carried out geometry optimizations of the different bulk perovskite phases using the ReaxFF. A complete comparison to DFT calculations and X-ray diffraction measurements[43] is summarized in Table S2. The results show minimal discrepancies (<2%). We highlight another validation by comparing the phase transition barrier for the inversion octahedral tilting in tetragonal $CsPbI_3$ in Figure 1d. The ReaxFF calculated barrier of 0.14 eV agrees well with our DFT result of 0.17 eV.

First, we use our I/Pb/Cs parameter set to investigate the phase evolution of $CsPbI_3$. We carry out ReaxFF MD simulations with AMS 2020[40] for a $CsPbI_3$ model system at several discrete temperatures between 100 and 700 K, as

https://doi.org/10.1021/acs.jpclett.1c01192
J. Phys. Chem. Lett. 2021, 12, 5519−5525

shown in Figure 2a (see Supporting Note 2 for details). Based on the evolution of the lattice vectors, we conclude that $CsPbI_3$ adopts the orthorhombic, tetragonal, and cubic phase from low to progressively higher temperatures,[43,44] with two phase transitions occurring at 350 ± 10 K and 450 ± 10 K. These phase transition temperatures are in qualitative agreement with experiments, with an underestimation of about 100 K for both transitions.[43] We attribute this underestimation to the slight overprediction of the lattice parameters during our simulations in comparison to experiments. We nevertheless find good agreement in the thermal expansion coefficient from ReaxFF (12.9×10^{-5} K^{-1}), which falls in the range of experimental values (11.8×10^{-5} K^{-1}[45] and 15.3×10^{-5} K^{-1}[43]).

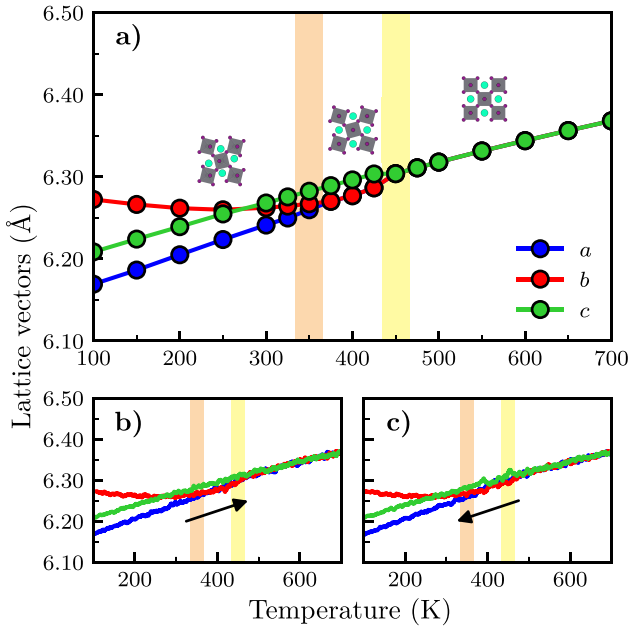

Figure 2. (a) The temperature dependence of the lattice vectors of $CsPbI_3$ from constant temperature simulations. (b, c) The evolution of the lattice vectors during gradual heating and cooling. The orange and yellow bars, respectively, indicate the phase transition temperatures for the orthorhombic to tetragonal and tetragonal to cubic phase transitions. In all figures the pseudocubic lattice vectors *a*, *b*, and *c* are used.

To investigate the reversibility of the phase evolution, a model system is subjected to a continuously changing temperature in Figure 2b and Figure 2c, respectively, showing the gradual heating and cooling. The similarity of the phase diagrams obtained from gradual heating and gradual cooling confirms that the phase transitions are reversible. We note that the ReaxFF MD simulations did not always show a complete reversibility (see Supporting Note 4). We attribute this to the formation of an orthorhombic structure that consists of multiple differently oriented domains. Such domains are stuck in different orthorhombic orientations and persist over time because of the lack of sufficient thermal energy. A similar phenomenon, i.e., the formation of various orthorhombic domains in $CsPbI_3$, has also been observed in experiments.[46]

After having investigated the overall phase behavior of $CsPbI_3$, we now analyze the dynamics of the lattice at different temperatures. For this we use a method outlined by Carignano et al.[47] with which the anharmonic character of the atomic fluctuations can be characterized. To do so, we define the geometrical parameter δ, which is the shortest distance from an I atom to the straight line interconnecting the two neighboring Pb atoms, as is shown in Figure 3a. The subsequent comparison of the probability distribution $P(\delta)$ from simulations against one derived for a harmonic approximation (see Supporting Note 6) allows for the qualitative description of the anharmonic character. We focus on a high-temperature cubic and a low-temperature orthorhombic phase, respectively, at 200 and 500 K, as shown in Figure 3b and Figure 3c,

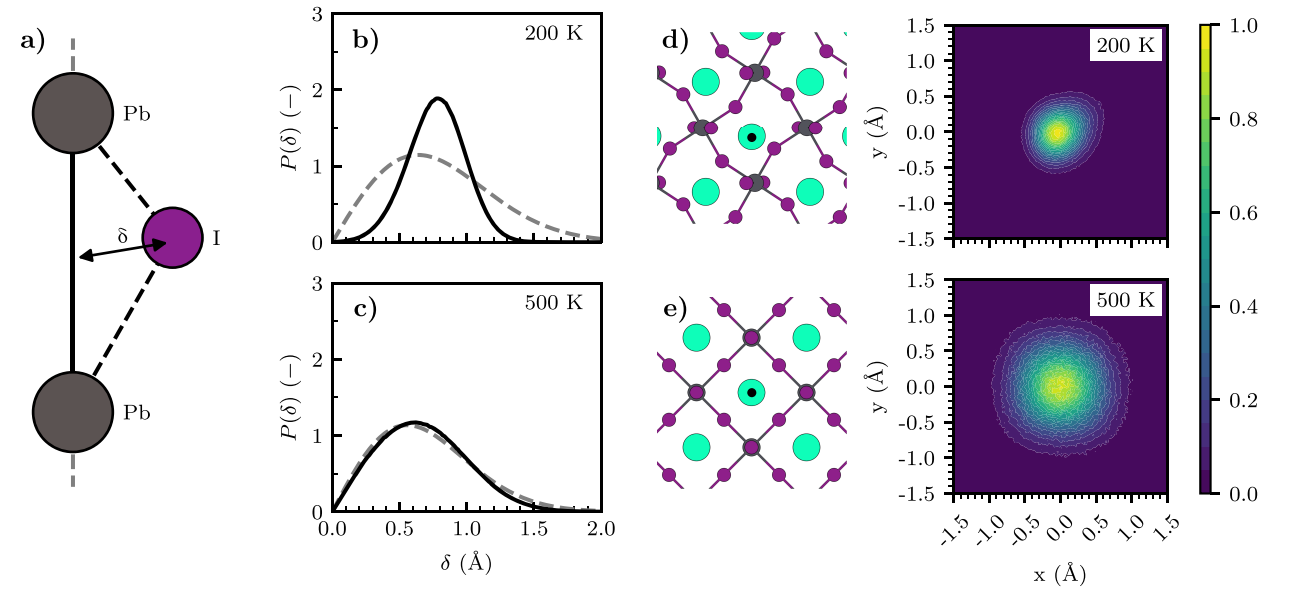

Figure 3. (a) Schematic representation of the geometrical parameter δ that is used an an indicator for the anharmonicity. (b, c) Comparison of the probability distributions of the geometrical parameter δ from simulations at 200 and 500 K (solid line) against the best fit of the harmonic model (dashed line). (d, e) Positional probability distribution of the Cs cations with respect to their average position in the perovskite lattice (black dot) from ReaxFF MD simulations at 200 and 500 K.

https://doi.org/10.1021/acs.jpclett.1c01192
J. Phys. Chem. Lett. 2021, 12, 5519−5525

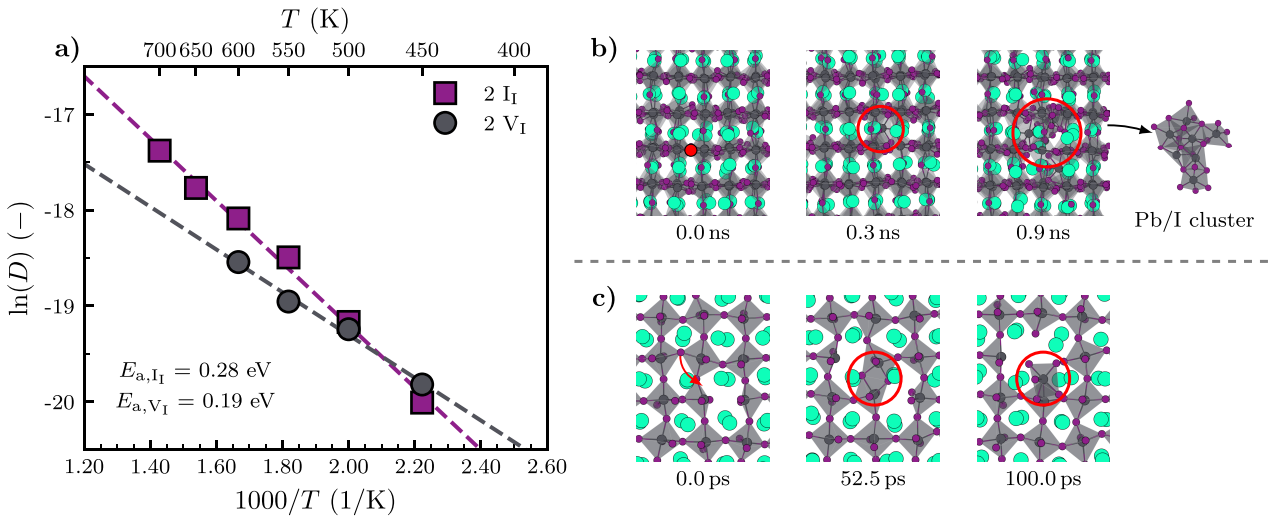

Figure 4. (a) Temperature evolution of the self-diffusion coefficients of iodine vacancies (V_I) and iodine interstitials (I_I). (b) Collection of snapshots of the different steps encountered during decomposition of $CsPbI_3$ in the presence of an iodine vacancy (red dot) at 600 K. The perovskite decomposes by forming a Pb/I cluster near the iodine vacancy. (c) Snapshots from the initial stages of the perovskite decomposition, showing the formation of an iodine Frenkel defect that subsequently results in a complex of edge-sharing metal halide octahedra that breaks away from its position in the lattice to form a Pb_xI_y complex.

respectively. By comparing the MD simulations and the best fit of the harmonic approximation, we observe that the harmonic approximation breaks down in both perovskite phases. The presence of this anharmonic character can be rationalized by Goldschmidt's principle of maximum cation−anion contact.[48,49] The tilting of the octahedra combined with a shift of the cation position allows for a better contact between the Cs ions and the surrounding iodine ions and thus stabilizes the perovskite structure. Interestingly, such behavior is highly sensitive to the temperature, with the largest degree of anharmonicity found at 200 K, which is significantly reduced at 500 K. We associate this reduction with the increase of the thermal energy, which induces a collective atom movement in the form of phonons,[9,50] causing the perovskite system to fluctuate between many distorted structures. At high temperature, such fluctuations become so fast that the time-averaged structure becomes cubic. We note that this decrease in the anharmonicity of the motion of the atoms is in line with the increase of symmetry when going from the orthorhombic to tetragonal and eventually cubic phase of $CsPbI_3$.

We next analyze the dynamics of the Cs cations in $CsPbI_3$ by constructing a positional probability distribution of the Cs cations. At 200 K, as shown in Figure 3d, we observe a directed motion of the cations, with a preferential movement in the positive *xy*-direction. We attribute this directional cation movement to the anharmonicity of the inorganic framework we observed above. We rationalize that this tendency of Cs cations to move away from the equilibrium positions can induce a structural instability, potentially converting to the nonperovskite yellow phase reported in experiments.[43,44,51] Our finding of Cs moving away from a stabilizing site to a destabilizing site is in line with experimental observations by Straus et al. from single-crystal X-ray diffraction measurements.[49] In contrast, the Cs distribution at 500 K, in Figure 3e, demonstrates that the directionality in motion of the Cs cations is lost, resulting in an isotropic distribution. This observation can readily be explained by the lack of any long-time local structure due to the rapid fluctuations of the metal halide framework. We suggest that the fluctuations of both the Cs cations and iodide anions result in good contacts between the two, stabilizing the perovskite phase at high temperatures.[43,45]

Another source of instability for halide perovskites is connected to the migration of ions. Two halide migration mechanisms, i.e., interstitial-assisted and vacancy-assisted mechanisms, have been proposed to be the major contributor to ion migration in the hybrid halide perovskite $MAPbI_3$.[24,52,53] Here, we investigate the relative importance of the two mechanisms in $CsPbI_3$. To do so, we carry out MD simulations to probe the temperature evolution of the self-diffusion coefficients of iodine vacancy and interstitial point defects. The simulations are done under atmospheric pressure at temperatures ranging from 450 to 700 K, from which the self-diffusion coefficients are extracted (see Supporting Note 2). The temperature evolution of the self-diffusion coefficients of both types of iodine point defects is shown in Figure 4a with a complete overview of the diffusion coefficients given in Table S3. Focusing on the self-diffusion coefficients, the information shows that in the investigated temperature range, where ReaxFF predicts $CsPbI_3$ to have a cubic phase, both types of defects exhibit similar rates of diffusion (10^{-9} to 10^{-8} cm^2 s^{-1}). The self-diffusion coefficients can be well described by a single Arrhenius relation. Therefore, we associate the migration of both point defects with a single activation energy of $E_{a,I_I} = 0.28$ eV for iodine interstitials and $E_{a,V_I} = 0.19$ eV for iodine vacancies, with a prefactor of $D_{0,I_I} = 3.1 \times 10^{-6}$ cm^2 s^{-1} for the former and $D_{0,V_I} = 3.6 \times 10^{-7}$ cm^2 s^{-1} for the latter. The relatively low energy barriers for both indicate that both ion migration processes readily occur in $CsPbI_3$. Specifically, our value for the energy barrier of iodine vacancy migration (0.19 eV) matches well with those observed for halogen vacancies in the inorganic perovskites $CsPbBr_3$ (0.25 eV) and $CsPbCl_3$ (0.29 eV) as measured by Mizusaki et al. using impedance spectroscopy.[54]

https://doi.org/10.1021/acs.jpclett.1c01192
J. Phys. Chem. Lett. 2021, 12, 5519−5525

Finally, we observe for high temperatures that the vacancy-rich $CsPbI_3$ systems have the tendency to result in the decomposition of the perovskite structure. In Figure 4b we show such an example, using snapshots of a ReaxFF simulation of $CsPbI_3$ with an iodine vacancy concentration of 3.0×10^{19} cm^{-3} at 600 K; however, a similar decomposition of the perovskite lattice is observed for concentrations as low as 4.5×10^{18} cm^{-3}. At the onset of the simulation, two iodine vacancies are dispersed in the perovskite phase. After some time, we observe that a lead species close to the iodine vacancy moves away from its position in the lattice, forming a locally Pb/I-rich domain. Further evolution of the system causes the Pb/I-rich region to grow in size, resulting in the formation of a Pb/I cluster. To elucidate the details of such a degradation process, an overview of the initial stages of the perovskite decomposition is shown in Figure 4c. The snapshots show that the degradation process begins with the formation of an iodine Frenkel defect close to the existing iodine vacancy; one iodine atom leaves its original position to create a vacancy and at the same time forms one iodine interstitial site. As a result of this, two octahedra are connected by the newly formed interstitial site, forming a complex of edge-sharing octahedra in which the PbI_x octahedra are only weakly bound to the rest of the perovskite lattice. Consequently, the lead species of either of these octahedra easily move away from their position in the lattice, forming a face-sharing Pb_xI_y complex, which subsequently grows to form a larger Pb/I cluster. Although the focus here is on the effects of iodine vacancies, we note that other types of vacancies (Pb and Cs) also resulted in the decomposition of the perovskite lattice through a similar mechanism (see Supporting Note 7), but at higher onset temperatures (700 K) than for iodine vacancies (600 K). This is because the involvement of Pb or Cs vacancies in the formation of iodine Frenkel defects is indirect, by making room in the perovskite lattice and facilitating the movement of the surrounding I species.

We hypothesize that such face-sharing Pb_xI_y complexes serve as the nucleation center for the decomposition of the perovskite structure, eventually leading to the decomposition of the halide perovskite into PbI_2. Our finding corroborates with recent observations from transmission electron microscopy experiments by Manekkathodi et al., in which PbI_2 nanoparticles are detected in the vicinity of lattice defects such a grain boundaries in mixed halide perovskites.[55] Moreover, our finding provides an atomistic interpretation of the fact that iodine-rich conditions can have a stabilizing effect on halide perovskites,[56] by inhibiting the formation of iodine vacancies that, from our ReaxFF simulations, appear to accelerate the degradation of the perovskites.

In summary, we develop and apply the first ReaxFF force field for studying dynamical processes associated with the stability issues of $CsPbI_3$. We demonstrate the phase instability at low temperature as a result of a combination of the dynamics of the Cs cations and the anharmonic nature of the fluctuations of the inorganic framework. The Cs cations prefer to locate at positions with good contact with the metal halide framework, which is facilitated by rapid dynamical fluctuations at high temperatures. When lowering the temperatures, Cs cations tend to move away from this preferential position, potentially resulting in the conversion of the perovskite phase to the nonperovskite phase. We also identify that iodine vacancies are detrimental to the stability of halide perovskites by facilitating the formation of iodine Frenkel defects and resulting in the decomposition of the perovskite lattice into Pb/I clusters. Our findings suggest that materials engineering strategies that mitigate the structural distortion (mixing with larger organic cations[57,58] or smaller anions such as the Br anion[59]) and reduce iodide vacancies (the synthesis of halide perovskites in I-rich conditions[60] or the inclusion of additives[61]) can improve the phase stability and defect related stability of $CsPbI_3$. We expect that the ReaxFF parameters in this work can be readily expanded to cover a broader range of perovskite compositions as well as their interactions with contact layers in devices, allowing for the study of reactive processes in realistic compositions relevant to the large-scale application of perovskite optoelectronics.

■ ASSOCIATED CONTENT

Supporting Information

The Supporting Information is available free of charge at https://pubs.acs.org/doi/10.1021/acs.jpclett.1c01192.

List of I/Pb/Cs ReaxFF parameters that were obtained from the parameter optimization procedure (TXT)

Overview of the benchmark of exchange-correlation functionals; summary of the computational methods used for the DFT calculations, ReaxFF MD simulations, and diffusion coefficient analysis; overview of the agreement between the ReaxFF force field and DFT calculations; comparison of two cooling runs of $CsPbI_3$; lattice vector analysis used for the phase diagram; harmonic approximation for perovskite lattice; snapshots of the decomposition mechanism for cesium and lead vacancies; tables of perovskite phase geometry optimizations and defect self-diffusion coefficients; figures that compare of variety of MD parameters for the phase diagram; and figure on the mean square displacement of species (PDF)

■ AUTHOR INFORMATION

Corresponding Author

Shuxia Tao − *Materials Simulation & Modelling, Department of Applied Physics and Center for Computational Energy Research, Department of Applied Physics, Eindhoven University of Technology, 5600 MB Eindhoven, The Netherlands;* orcid.org/0000-0002-3658-8497; Email: s.x.tao@tue.nl

Authors

Mike Pols − *Materials Simulation & Modelling, Department of Applied Physics, Laboratory of Inorganic Materials Chemistry, Schuit Institute of Catalysis, Department of Chemical Engineering and Chemistry, and Center for Computational Energy Research, Department of Applied Physics, Eindhoven University of Technology, 5600 MB Eindhoven, The Netherlands;* orcid.org/0000-0002-1068-9599

José Manuel Vicent-Luna − *Materials Simulation & Modelling, Department of Applied Physics and Center for Computational Energy Research, Department of Applied Physics, Eindhoven University of Technology, 5600 MB Eindhoven, The Netherlands;* orcid.org/0000-0001-8712-5591

Ivo Filot − *Laboratory of Inorganic Materials Chemistry, Schuit Institute of Catalysis, Department of Chemical Engineering and Chemistry and Center for Computational*

Energy Research, Department of Applied Physics, Eindhoven University of Technology, 5600 MB Eindhoven, The Netherlands; orcid.org/0000-0003-1403-8379

Adri C. T. van Duin − *Department of Mechanical Engineering, Pennsylvania State University, University Park, Pennsylvania 16802, United States;* orcid.org/0000-0002-3478-4945

Complete contact information is available at: https://pubs.acs.org/10.1021/acs.jpclett.1c01192

Notes

The authors declare no competing financial interest.

■ ACKNOWLEDGMENTS

M.P. and S.T. acknowledge funding by the Computational Sciences for Energy Research (CSER) tenure track program of Shell and NWO (project no. 15CST04-2); J.M.V.L. and S.T. acknowledge NWO START-UP support from The Netherlands.

■ REFERENCES

(1) Green, M. A.; Ho-Baillie, A.; Snaith, H. J. The Emergence of Perovskite Solar Cells. *Nat. Photonics* **2014**, *8*, 506−514.
(2) Snaith, H. J. Present Status and Future Prospects of Perovskite Photovoltaics. *Nat. Mater.* **2018**, *17*, 372−376.
(3) Kojima, A.; Teshima, K.; Shirai, Y.; Miyasaka, T. Organometal Halide Perovskites as Visible-Light Sensitizers for Photovoltaic Cells. *J. Am. Chem. Soc.* **2009**, *131*, 6050−6051.
(4) National Renewable Energy Laboratory. Best Research-Cell Efficiency Chart. NREL: 2020; https://www.nrel.gov/pv/cell-efficiency.html (accessed 2021).
(5) Poglitsch, A.; Weber, D. Dynamic Disorder in Methylammoniumtrihalogenoplumbates (II) Observed by Millimeter-Wave Spectroscopy. *J. Chem. Phys.* **1987**, *87*, 6373−6378.
(6) Mashiyama, H.; Kurihara, Y.; Azetsu, T. Disordered Cubic Perovskite Structure of $CH_3NH_3PbX_3$ (X = Cl, Br, I). *J. Korean Phys. Soc.* **1998**, *32*, 156−158.
(7) Feng, J. Mechanical Properties of Hybrid Organic-Inorganic $CH_3NH_3BX_3$ (B = Sn, Pb; X = Br, I) Perovskites for Solar Cell Absorbers. *APL Mater.* **2014**, *2*, 081801.
(8) Sun, S.; Fang, Y.; Kieslich, G.; White, T. J.; Cheetham, A. K. Mechanical Properties of Organic−Inorganic Halide Perovskites, $CH_3NH_3PbX_3$ (X = I, Br and Cl), by Nanoindentation. *J. Mater. Chem. A* **2015**, *3*, 18450−18455.
(9) Glinka, Y. D.; Cai, R.; Gao, X.; Wu, D.; Chen, R.; Sun, X. W. Structural Phase Transitions and Photoluminescence Mechanism in a Layer of 3D Hybrid Perovskite Nanocrystals. *AIP Adv.* **2020**, *10*, 065028.
(10) Niu, G.; Guo, X.; Wang, L. Review of Recent Progress in Chemical Stability of Perovskite Solar Cells. *J. Mater. Chem. A* **2015**, *3*, 8970−8980.
(11) Wang, D.; Wright, M.; Elumalai, N. K.; Uddin, A. Stability of Perovskite Solar Cells. *Sol. Energy Mater. Sol. Cells* **2016**, *147*, 255−275.
(12) Correa-Baena, J.-P.; Saliba, M.; Buonassisi, T.; Grätzel, M.; Abate, A.; Tress, W.; Hagfeldt, A. Promises and Challenges of Perovskite Solar Cells. *Science* **2017**, *358*, 739−744.
(13) Park, B.-w.; Seok, S. I. Intrinsic Instability of Inorganic−Organic Hybrid Halide Perovskite Materials. *Adv. Mater.* **2019**, *31*, 1805337.
(14) Qiu, Z.; Li, N.; Huang, Z.; Chen, Q.; Zhou, H. Recent Advances in Improving Phase Stability of Perovskite Solar Cells. *Small Methods* **2020**, *4*, 1900877.
(15) Stranks, S. D.; Burlakov, V. M.; Leijtens, T.; Ball, J. M.; Goriely, A.; Snaith, H. J. Recombination Kinetics in Organic-Inorganic Perovskites: Excitons, Free Charge, and Subgap States. *Phys. Rev. Appl.* **2014**, *2*, 034007.
(16) Draguta, S.; Thakur, S.; Morozov, Y. V.; Wang, Y.; Manser, J. S.; Kamat, P. V.; Kuno, M. Spatially Non-Uniform Trap State Densities in Solution-Processed Hybrid Perovskite Thin Films. *J. Phys. Chem. Lett.* **2016**, *7*, 715−721.
(17) Carrillo, J.; Guerrero, A.; Rahimnejad, S.; Almora, O.; Zarazua, I.; Mas-Marza, E.; Bisquert, J.; Garcia-Belmonte, G. Ionic Reactivity at Contacts and Aging of Methylammonium Lead Triiodide Perovskite Solar Cells. *Adv. Energy Mater.* **2016**, *6*, 1502246.
(18) Li, J.; Dong, Q.; Li, N.; Wang, L. Direct Evidence of Ion Diffusion for the Silver-Electrode-Induced Thermal Degradation of Inverted Perovskite Solar Cells. *Adv. Energy Mater.* **2017**, *7*, 1602922.
(19) Di Girolamo, D.; Phung, N.; Kosasih, F. U.; Di Giacomo, F.; Matteocci, F.; Smith, J. A.; Flatken, M. A.; Köbler, H.; Turren Cruz, S. H.; Mattoni, A.; et al. Ion Migration-Induced Amorphization and Phase Segregation as a Degradation Mechanism in Planar Perovskite Solar Cells. *Adv. Energy Mater.* **2020**, *10*, 2000310.
(20) Mosconi, E.; Azpiroz, J. M.; De Angelis, F. Ab Initio Molecular Dynamics Simulations of Methylammonium Lead Iodide Perovskite Degradation by Water. *Chem. Mater.* **2015**, *27*, 4885−4892.
(21) Zhang, L.; Sit, P. H.-L. Ab Initio Static and Dynamic Study of $CH_3NH_3PbI_3$ Degradation in the Presence of Water, Hydroxyl Radicals, and Hydroxide Ions. *RSC Adv.* **2016**, *6*, 76938−76947.
(22) Zheng, C.; Rubel, O. Unraveling the Water Degradation Mechanism of $CH_3NH_3PbI_3$. *J. Phys. Chem. C* **2019**, *123*, 19385−19394.
(23) Mattoni, A.; Filippetti, A.; Saba, M. I.; Delugas, P. Methylammonium Rotational Dynamics in Lead Halide Perovskite by Classical Molecular Dynamics: The Role of Temperature. *J. Phys. Chem. C* **2015**, *119*, 17421−17428.
(24) Delugas, P.; Caddeo, C.; Filippetti, A.; Mattoni, A. Thermally Activated Point Defect Diffusion in Methylammonium Lead Trihalide: Anisotropic and Ultrahigh Mobility of Iodine. *J. Phys. Chem. Lett.* **2016**, *7*, 2356−2361.
(25) Phung, N.; Al-Ashouri, A.; Meloni, S.; Mattoni, A.; Albrecht, S.; Unger, E. L.; Merdasa, A.; Abate, A. The Role of Grain Boundaries on Ionic Defect Migration in Metal Halide Perovskites. *Adv. Energy Mater.* **2020**, *10*, 1903735.
(26) Caddeo, C.; Saba, M. I.; Meloni, S.; Filippetti, A.; Mattoni, A. Collective Molecular Mechanisms in the $CH_3NH_3PbI_3$ Dissolution by Liquid Water. *ACS Nano* **2017**, *11*, 9183−9190.
(27) Rathnayake, P. V. G. M.; Bernardi, S.; Widmer-Cooper, A. Evaluation of the AMOEBA Force Field for Simulating Metal Halide Perovskites in the Solid State and in Solution. *J. Chem. Phys.* **2020**, *152*, 024117.
(28) Balestra, S. R. G.; Vicent-Luna, J. M.; Calero, S.; Tao, S.; Anta, J. A. Efficient Modelling of Ion Structure and Dynamics in Inorganic Metal Halide Perovskites. *J. Mater. Chem. A* **2020**, *8*, 11824−11836.
(29) van Duin, A. C. T.; Dasgupta, S.; Lorant, F.; Goddard, W. A. ReaxFF: A Reactive Force Field for Hydrocarbons. *J. Phys. Chem. A* **2001**, *105*, 9396−9409.
(30) Chenoweth, K.; van Duin, A. C. T.; Persson, P.; Cheng, M.-J.; Oxgaard, J.; Goddard, W. A. Development and Application of a ReaxFF Reactive Force Field for Oxidative Dehydrogenation on Vanadium Oxide Catalysts. *J. Phys. Chem. C* **2008**, *112*, 14645−14654.
(31) Senftle, T. P.; Hong, S.; Islam, M. M.; Kylasa, S. B.; Zheng, Y.; Shin, Y. K.; Junkermeier, C.; Engel-Herbert, R.; Janik, M. J.; Aktulga, H. M.; et al. The ReaxFF Reactive Force-Field: Development, Applications and Future Directions. *npj Comput. Mater.* **2016**, *2*, 1−14.
(32) Perdew, J. P.; Burke, K.; Ernzerhof, M. Generalized Gradient Approximation Made Simple. *Phys. Rev. Lett.* **1996**, *77*, 3865−3868.
(33) Perdew, J. P.; Burke, K.; Ernzerhof, M. Generalized Gradient Approximation Made Simple [Phys. Rev. Lett. 77, 3865 (1996)]. *Phys. Rev. Lett.* **1997**, *78*, 1396−1396.

(34) Grimme, S.; Ehrlich, S.; Goerigk, L. Effect of the Damping Function in Dispersion Corrected Density Functional Theory. *J. Comput. Chem.* **2011**, *32*, 1456−1465.
(35) Kresse, G.; Hafner, J. Ab Initio Molecular Dynamics for Liquid Metals. *Phys. Rev. B: Condens. Matter Mater. Phys.* **1993**, *47*, 558−561.
(36) Kresse, G.; Hafner, J. Ab Initio Molecular-Dynamics Simulation of the Liquid-Metal-Amorphous-Semiconductor Transition in Germanium. *Phys. Rev. B: Condens. Matter Mater. Phys.* **1994**, *49*, 14251−14269.
(37) Kresse, G.; Furthmüller, J. Efficiency of Ab-Initio Total Energy Calculations for Metals and Semiconductors Using a Plane-Wave Basis Set. *Comput. Mater. Sci.* **1996**, *6*, 15−50.
(38) Kresse, G.; Furthmüller, J. Efficient Iterative Schemes for Ab Initio Total-Energy Calculations Using a Plane-Wave Basis Set. *Phys. Rev. B: Condens. Matter Mater. Phys.* **1996**, *54*, 11169−11186.
(39) Iype, E.; Hütter, M.; Jansen, A. P. J.; Nedea, S. V.; Rindt, C. C. M. Parameterization of a Reactive Force Field Using a Monte Carlo Algorithm. *J. Comput. Chem.* **2013**, *34*, 1143−1154.
(40) AMS 2020, SCM, Theoretical Chemistry, Vrije Universiteit, Amsterdam, The Netherlands, 2020.
(41) Fedkin, M. V.; Shin, Y. K.; Dasgupta, N.; Yeon, J.; Zhang, W.; van Duin, D.; van Duin, A. C. T.; Mori, K.; Fujiwara, A.; Machida, M.; et al. Development of the ReaxFF Methodology for Electrolyte−Water Systems. *J. Phys. Chem. A* **2019**, *123*, 2125−2141.
(42) Fantauzzi, D.; Mueller, J. E.; Sabo, L.; van Duin, A. C. T.; Jacob, T. Surface Buckling and Subsurface Oxygen: Atomistic Insights into the Surface Oxidation of Pt(111). *ChemPhysChem* **2015**, *16*, 2797−2802.
(43) Marronnier, A.; Roma, G.; Boyer-Richard, S.; Pedesseau, L.; Jancu, J.-M.; Bonnassieux, Y.; Katan, C.; Stoumpos, C. C.; Kanatzidis, M. G.; Even, J. Anharmonicity and Disorder in the Black Phases of Cesium Lead Iodide Used for Stable Inorganic Perovskite Solar Cells. *ACS Nano* **2018**, *12*, 3477−3486.
(44) Stoumpos, C. C.; Kanatzidis, M. G. The Renaissance of Halide Perovskites and Their Evolution as Emerging Semiconductors. *Acc. Chem. Res.* **2015**, *48*, 2791−2802.
(45) Trots, D. M.; Myagkota, S. V. High-Temperature Structural Evolution of Caesium and Rubidium Triiodoplumbates. *J. Phys. Chem. Solids* **2008**, *69*, 2520−2526.
(46) Bertolotti, F.; Protesescu, L.; Kovalenko, M. V.; Yakunin, S.; Cervellino, A.; Billinge, S. J. L.; Terban, M. W.; Pedersen, J. S.; Masciocchi, N.; Guagliardi, A. Coherent Nanotwins and Dynamic Disorder in Cesium Lead Halide Perovskite Nanocrystals. *ACS Nano* **2017**, *11*, 3819−3831.
(47) Carignano, M. A.; Aravindh, S. A.; Roqan, I. S.; Even, J.; Katan, C. Critical Fluctuations and Anharmonicity in Lead Iodide Perovskites from Molecular Dynamics Supercell Simulations. *J. Phys. Chem. C* **2017**, *121*, 20729−20738.
(48) Goldschmidt, V. M. Crystal Structure and Chemical Constitution. *Trans. Faraday Soc.* **1929**, *25*, 253−283.
(49) Straus, D. B.; Guo, S.; Abeykoon, A. M.; Cava, R. J. Understanding the Instability of the Halide Perovskite $CsPbI_3$ through Temperature-Dependent Structural Analysis. *Adv. Mater.* **2020**, *32*, 2001069.
(50) Whitfield, P. S.; Herron, N.; Guise, W. E.; Page, K.; Cheng, Y. Q.; Milas, I.; Crawford, M. K. Structures, Phase Transitions and Tricritical Behavior of the Hybrid Perovskite Methyl Ammonium Lead Iodide. *Sci. Rep.* **2016**, *6*, 1−16.
(51) Stoumpos, C. C.; Malliakas, C. D.; Kanatzidis, M. G. Semiconducting Tin and Lead Iodide Perovskites with Organic Cations: Phase Transitions, High Mobilities, and Near-Infrared Photoluminescent Properties. *Inorg. Chem.* **2013**, *52*, 9019−9038.
(52) Azpiroz, J. M.; Mosconi, E.; Bisquert, J.; De Angelis, F. Defect Migration in Methylammonium Lead Iodide and Its Role in Perovskite Solar Cell Operation. *Energy Environ. Sci.* **2015**, *8*, 2118−2127.
(53) Yang, J.-H.; Yin, W.-J.; Park, J.-S.; Wei, S.-H. Fast Self-Diffusion of Ions in $CH_3NH_3PbI_3$: the Interstiticaly Mechanism Versus Vacancy-Assisted Mechanism. *J. Mater. Chem. A* **2016**, *4*, 13105−13112.
(54) Mizusaki, J.; Arai, K.; Fueki, K. Ionic Conduction of the Perovskite-Type Halides. *Solid State Ionics* **1983**, *11*, 203−211.
(55) Manekkathodi, A.; Marzouk, A.; Ponraj, J.; Belaidi, A.; Ashhab, S. Observation of Structural Phase Transitions and PbI_2 Formation During the Degradation of Triple-Cation Double-Halide Perovskites. *ACS Appl. Energy Mater.* **2020**, *3*, 6302−6309.
(56) Kye, Y.-H.; Yu, C.-J.; Jong, U.-G.; Ri, K.-C.; Kim, J.-S.; Choe, S.-H.; Hong, S.-N.; Li, S.; Wilson, J. N.; Walsh, A. Vacancy-Driven Stabilization of the Cubic Perovskite Polymorph of $CsPbI_3$. *J. Phys. Chem. C* **2019**, *123*, 9735−9744.
(57) Zhang, J.; Yang, L.; Zhong, Y.; Hao, H.; Yang, M.; Liu, R. Improved Phase Stability of the $CsPbI_3$ Perovskite via Organic Cation Doping. *Phys. Chem. Chem. Phys.* **2019**, *21*, 11175−11180.
(58) Liu, D.; Zha, W.; Guo, Y.; Sa, R. Insight into the Improved Phase Stability of $CsPbI_3$ from First-Principles Calculations. *ACS Omega* **2020**, *5*, 893−896.
(59) Sutton, R. J.; Eperon, G. E.; Miranda, L.; Parrott, E. S.; Kamino, B. A.; Patel, J. B.; Hörantner, M. T.; Johnston, M. B.; Haghighirad, A. A.; Moore, D. T.; et al. Bandgap-Tunable Cesium Lead Halide Perovskites with High Thermal Stability for Efficient Solar Cells. *Adv. Energy Mater.* **2016**, *6*, 1502458.
(60) Eperon, G. E.; Paternó, G. M.; Sutton, R. J.; Zampetti, A.; Haghighirad, A. A.; Cacialli, F.; Snaith, H. J. Inorganic Caesium Lead Iodide Perovskite Solar Cells. *J. Mater. Chem. A* **2015**, *3*, 19688−19695.
(61) Guo, Y.; Liu, H.; Li, W.; Zhu, L.; Chen, H. Additive Engineering Toward High-Performance $CsPbI_3$ Perovskite Solar Cells. *Sol. RRL* **2020**, *4*, 2000380.

https://doi.org/10.1021/acs.jpclett.1c01192
J. Phys. Chem. Lett. 2021, 12, 5519−5525